Inorg. Chem. **2006**, *45*, 1861−1870

Photochemical and Time Resolved Spectroscopic Studies of Intermediates Relevant to Iridium-Catalyzed Methanol Carbonylation: Photoinduced CO Migratory Insertion

Maurizio Volpe,[†] Guang Wu,[†] Alexei Iretskii,[†,‡] and Peter C. Ford*[,†]

Department of Chemistry and Biochemistry, University of California, Santa Barbara, California 93106-9510, and Department of Chemistry, Lake Superior State University, 650 West Easterday Avenue, Sault Sainte Marie, Michigan 49783

Received October 20, 2005

Photoreaction, time-resolved infrared (TRIR), and DFT studies were utilized to probe transformations between iridium complexes with possible relevance to the mechanisms of the iridium/iodide-catalyzed methanol carbonylation to acetic acid. Solution-phase continuous and laser flash photolysis of the tetraphenylarsonium salt of the *fac*-$[CH_3Ir(CO)_2I_3]^-$ anion (**1a**) under excess carbon monoxide resulted in migratory insertion to give the acyl complex ion *mer,trans*-$[Ir(C(O)CH_3)(CO)_2I_3]^-$ (**2a**). The latter was isolated as its $AsPh_4^+$ salt, and its X-ray crystal structure was determined. TRIR spectra indicate that several transients are generated upon flash photolysis of **1a**. The principal photoreaction is CO dissociation, and this is proposed to generate the isomeric complexes *fac*-$[CH_3Ir(CO)(Sol)I_3]^-$ ($\mathbf{I}_{CO}$(*fac*), Sol = solvent) and *mer,trans*-$[CH_3Ir(CO)(Sol)I_3]^-$ ($\mathbf{I}_{CO}$(*mer*)). $\mathbf{I}_{CO}$(*fac*) reacts with CO to regenerate **1a** with a second-order rate constant (k_{CO}) $\sim 2.5 \times 10^7$ M^{-1} s^{-1} in ambient dichloroethane, while $\mathbf{I}_{CO}$(*mer*) is the apparent precursor to **2a**. Kinetics studies indicate the photoinduced formation of a third intermediate ($\mathbf{I}_M$), hypothesized to be the anionic acyl complex *fac*-$[Ir(C(O)CH_3)(CO)(Sol)I_3]^-$. In the absence of added CO, these intermediates undergo dimerization to form a mixture of isomers with the apparent formula $[Ir(C(O)CH_3)(CO)I_3]_2^{2-}$. One of these dimers was isolated as the $AsPh_4^+$ salt, and the crystal structure was determined. Addition of excess pyridine to a solution of the dimers gave the neutral complex *mer,trans*-$[Ir(C(O)CH_3)(CO)(py)_2I_2]$, which was characterized by FTIR, NMR, and X-ray crystallography. These transformations, especially the unprecedented photoinduced CO insertion reaction, are discussed and interpreted in terms of the factors favoring migratory insertion dynamics.

Introduction

The carbonylation of methanol to acetic acid by a rhodium/iodide catalyst (Monsanto process) is one of the most successful industrial applications of homogeneous catalysis.[1] More recently, a methanol carbonylation process based on a promoted iridium/iodide catalyst (Cativa process) has been commercialized.[2] The catalytic mechanism that has been outlined for this process involves participation of various iodo iridium carbonyl species in interlocking "neutral" and "anionic" cycles.[3,4] Quantitative investigations point to the "anionic" cycle illustrated by Scheme 1 as being predominant under conditions of commercial catalysis.[3,4]

A key species in Scheme 1 is the methyl iridium complex *fac*-$[CH_3Ir(CO)_2I_3]^-$ (**1a**), the resting state of this cycle. According to the accepted mechanism, the steps leading to

* To whom correspondence should be addressed. E-mail: ford@chem.ucsb.edu.
[†] University of California, Santa Barbara.
[‡] Lake Superior State University.

(1) Parshall, G. W.; Ittel, S. D. *Homogeneous Catalysis*; John Wiley and Sons: New York, 1992.
(2) (a) *Chem. Br.* **1996**, *32*, 7. (b) Sunley, G. J.; Watson, D. J. *Catal. Today.* **2000**, *58*, 293−307.
(3) Forster, D. *J. Chem. Soc., Dalton Trans.* **1979**, 1639−1645.
(4) (a) Bassetti, M.; Monti, D.; Haynes, A.; Pearson, J. M.; Stanbridge, I. A.; Maitlis, P. M. *Gazz. Chim. Ital.* **1992**, *122*, 391−393. (b) Pearson, J. M.; Haynes, A.; Morris, G. E.; Sunley, G. J.; Maitlis, P. M. *J. Chem. Soc., Chem. Commun.* **1995**, 1045−1046. (c) Maitlis, P. M.; Haynes, A.; Sunley, G. J.; Howard, M. *J. Chem. Soc., Dalton Trans.* **1996**, 2187−2196. (d) Ghaffar, T.; Adams, H.; Maitlis, P. M.; Sunley, G. J.; Baker, M. J.; Haynes, A.; Howard, M. *Chem. Commun.* **1998**, 1023−1024. (e) Haynes, A.; Maitlis, P. M.; Morris, G. E.; Sunley G. J.; Adams, H.; Badger, P. W.; Bowers, C. M.; Cook, D. B.; Elliott, P. I. P.; Ghaffar, T.; Green, H.; Griffin, T. R.; Payne, M.; Pearson, J. M.; Taylor, M. J.; Vickers, P. W.; Watt, R. J. *J. Am. Chem. Soc.* **2004**, *126*, 2847−2861.

10.1021/ic0513033 CCC: $33.50
Published on Web 01/10/2006

Scheme 1. Anionic Cycle of Proposed Mechanism for Ir/I−Catalyzed Methanol Carbonylation

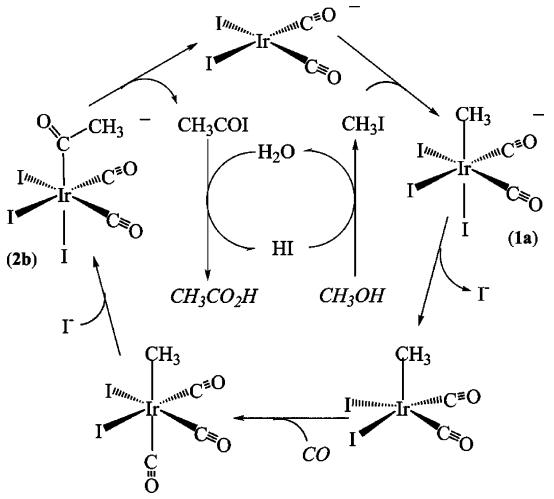

CO migratory insertion to give an acyl intermediate are rate limiting.[4a,c] In nonpolar media, this transformation is dramatically accelerated by added methanol and Lewis acids, is strongly inhibited by iodide salts such as $[Bu_4N]I$,[4b] and is promoted by neutral ruthenium iodo carbonyls and main-group iodides (e.g., InI_3, GaI_3, SnI_2, and ZnI_2).[4e] These observations were interpreted in terms of **1a** being activated by iodide scavengers that promote transformation under CO to the neutral *fac*-tricarbonyl complex $[CH_3Ir(CO)_3I_2]$, which undergoes methyl migration and I^- addition to form the acyl complex ion *fac*-$[Ir(C(O)CH_3)(CO)_2I_3]^-$ (**2b**). This reactivity has been attributed to enhanced electrophilicity of the cis carbonyl, owing to competition for metal d electrons from the other COs.[4d,e,5] Reductive elimination from **2b** and hydrolysis of the resulting acetyl iodide leads to acetic acid formation.

The goal of the present study was to utilize photochemical techniques to generate and time-resolved spectroscopy to interrogate intermediates possibly relevant to methanol carbonylation promoted by iridium salts. In the course of this investigation, we have demonstrated that irradiation of **1a** promotes an unprecedented photoinduced CO migratory insertion to give the stable acetyl complex ion *mer,trans*-$[Ir(C(O)CH_3)(CO)_2I_3]^-$ (**2a**), which was isolated as the $AsPh_4^+$ salt and structurally characterized. Here we describe the characterization of various transient and stable species formed under various conditions and discuss the possible relevance of these with regard to catalytic pathways involving iridium iodo carbonyl complexes.

Experimental Section

Materials. Iridium trichloride hydrate, tetraphenylarsonium chloride, and iodomethane were purchased from Aldrich and used without further purification. The solvents used in these experiments (1,2-dichoroethane (DCE), dichloromethane, acetonitrile, and tetrahydrofuran (THF)) were purified and dried following standard distillation procedures.[6] Deuterated acetonitrile and dichloromethane were purchased from Cambridge Isotope Laboratories and used without any further purification. Gases were obtained from Praxair.

Photolysis Procedures. The solutions studied by continuous and laser flash photolysis techniques were contained in a gastight flask fused to a quartz cell, in a CaF_2 IR cell sealed with serum caps, or in the flow system described below. The sample concentration for the measurement was typically 1−3 mM except for bulk photolysis reactions where higher concentrations were used. The solutions were deaerated by entrainment with argon or carbon monoxide with three freeze−pump−thaw cycles then equilibrated under Ar or CO (various P_{CO}).

The time-resolved infrared spectrometer and its applications to the reactions of metal carbonyl intermediates in migratory insertion reactions have been described previously.[7] In the current configuration, the IR probe is generated by a lead salt diode laser with a single longitudinal mode selected by a CVI Digikrom Model 240 monochromator. The probe beam was overlapped at the plane of the infrared cell with a 355 nm pump pulse from a Lumonics HY600 Nd:YAG laser. The high-pressure/variable-temperature (HP/VT) flow system assembled at UCSB[7g] allowed for the equilibration of sample solutions for time-resolved infrared (TRIR) experiments with various pressures of CO at the desired temperatures and provided a steady flow of fresh sample solution to a CaF_2 IR cell for photolysis experiments.

Continuous photolysis experiments were conducted using standard procedures[8] in a darkroom. The excitation source was a 200 W high-pressure mercury lamp mounted on an Oriel optical train (UVP) with intensity regulation by an internal feedback loop. The light from this source was first passed through an IR filter, followed by neutral density filters to reduce intensity, and an interference filter to isolate the mercury line at 366 nm. A lens was used to focus the light onto the sample, and the solution was stirred continuously. Ferrioxalate actinometry was used to evaluate light intensities.[8a,b] The sample was irradiated for the specific period, and the reaction progress was monitored by UV−visible and FTIR spectroscopy. Quantum yields were determined by fitting plots of incremental quantum yields, Φ_i (first 10−30% of the reaction), for absorbance changes vs percent reaction with a linear equation.[8c,d] The *y* intercept is the photoreaction quantum yield, Φ. Experiments were carried out multiple times to ensure reproducibility.

Bulk photolysis reactions were carried out by using standard gastight Schlenk flasks or gastight NMR tubes for experiments in deuterated solvent. The apparatus used is an ACE Glass photochemical safety UV cabinet model 7836-20 and a 200 W mercury lamp immersed in a quartz well with flowing water for cooling and for IR filtering.

(5) (a) Similar enhanced electrophilicity of coordinated CO was used to interpret [CO] effects on the water gas shift catalytic activity of rhodium halo carbonyl complexes in aqueous amine solutions.[5b,c] (b) Lima Neto, B. S.; Ford, K. H.; Pardey, A. J.; Rinker, R. J.; Ford, P. C. *Inorg. Chem*. **1991**, *30*, 3837−3842. (c) Ford, P. C.; Rockicki, A. *Adv. Organomet. Chem*. **1988**, *28*, 139−217.

(6) Riddick, J. A.; Bunger, W. B.; Sakano, T. K. *Organic Solvents Physical Properties and Methods of Purification*, 4th ed.; John Wiley and Sons: New York, 1986; Vol. II.

(7) (a) Di Benedetto, J. A.; Ryba, D. W.; Ford, P. C. *Inorg. Chem.* **1989**, *28*, 3503−3507. (b) Boese, W. T.; Ford, P. C. *J. Am. Chem. Soc.* **1995**, *117*, 8381−8391. (c) Massick, S.; Rabor, J.; Elbers, S.; Marhenke, J.; Bernhard, S.; Schoonover, J.; Ford, P. C. *Inorg. Chem.* **2000,** *39*, 3098−3106. (d) Massick, S. M.; Mertens, V.; Jon Marhenke, J.; Ford, P. C. *Inorg. Chem.*, **2002**, *41*, 3553−3559. (e) Massick, S. M.; Büttner, T.; Ford, P. C. *Inorg. Chem.* **2003**, *42*, 575−580. (f) Ford, P. C.; Massick, S. M. *Coord. Chem. Rev.* **2002**, *226*, 39−46. (g) Massick, S. M.; Ford, P. C. *Organometallics* **1999**, *18*, 4362−4366.

(8) (a) Calvert, J. G.; Pitts, J. N. *Photochemistry*; John Wiley and Sons: New York, 1967; pp 783−786. (b) Malouf, G.; Ford, P. C. *J. Am. Chem. Soc.* **1977**, *99*, 7213−7221. (c) Chaisson, D. A.; Hintze, R. E.; Stuemer, D. H.; Petersen, J. D. Mcdonald, D. P.; Ford, P. C. *J. Am. Chem. Soc*. **1972**, *94*, 6665−6673. (d) Works, C. F.; Jocher, C. J.; Bart, G. D.; Bu, X.; Ford, P. C. *Inorg. Chem.* **2002**, *41*, 3728−3736.

(9) (a) Forster, D. *Inorg. Nucl. Chem. Lett.* **1969**, 5, 433−436. (b) Forster, D. *Inorg. Chem,*. **1972**, *11*, 473−475.

Instrumentation. UV−visible spectra were recorded using a Hewlett-Packard diode array spectrophotometer or a Shimadzu model 2401PC spectrophotometer. Infrared spectra were obtained using a BioRad model FTS 60 SPC 3200 FTIR spectrometer. ESI-MS were acquired on a VG Fision Platform II single-quadrupole mass spectrometer with an electrospray ionization source and a Fision Masslink data system. All samples were diluted in HPLC grade acetonitrile immediately prior to measurement. NMR spectra were registered on Varian 200 and 400 MHz spectrometers in CD_2Cl_2 (5.32 ppm) or CD_3CN (1.94 ppm). Solid-state MAS NMR spectra were recorded at room temperature on a Bruker 300 MHz Avance Spectrometer with a 4 mm broadband MAS probe double tuned to ^1H(300.1 MHz) and ^{13}C(75.5 MHz). A spinning speed of 1 kHz was used in the experiments.

Syntheses. *fac*-$[CH_3Ir(CO)_2I_3][AsPh_4]$ ($AsPh_4^+$ salt of **1a).** This compound was prepared from *cis*-$[Ir(CO)_2I_2][Ph_4As]$ according to literature methods.[4e,9] ESI-MS: 644.69 *m*/*z* (M^-). IR (CH_2Cl_2) ν(CO) in cm^{-1}: 2098 ($\epsilon = 1.9 \times 10^3\ M^{-1}\ cm^{-1}$), 2046 ($1.3 \times 10^3$). ^1H NMR (CD_2Cl_2): δ 2.1 (s, 3H, CH_3), δ 7.6−7.9 (m, 20H, Ph_4-As). ^{13}C NMR (CD_2Cl_2): δ 156.4 (*C*O), 135.5, 133.5, 131.9 (Ph, *C*H), 121.0 (Ph, As*C*), −16.0 (*C*H_3).

***mer,trans*-[Ir(C(O)CH$_3$)(CO)$_2$I$_3$][AsPh$_4$] ($AsPh_4^+$ salt of 2a).** *fac*-$[CH_3Ir(CO)_2I_3][AsPh_4]$ (205 mg, 0.2 mM) was dissolved in 50 mL of deaerated CH_2Cl_2, and the solution equilibrated with CO at atmospheric pressure for 1 h. The solution was then subjected to bulk photolysis for 2 h until complete reaction of **1a** was achieved (the course of reaction was followed by FTIR and ESI-MS). The volume of the solution was reduced to about 5 mL in vacuo, and crystallization of the $AsPh_4^+$ salt of **2a** achieved by layering the CH_2Cl_2 solution with diethyl ether. The orange crystals were separated, washed with diethyl ether, and slowly dried under flowing nitrogen. Yield: 140 mg (68%). Anal. Calcd for ($C_{28}H_{23}O_3IrI_3As$): C, 31.87; H, 2.20. Found: C, 31.93; H, 2.10. ESI-MS: 672.70 *m*/*z* (M^-). IR (CH_2Cl_2) ν(CO) in cm^{-1}: 2064 ($\epsilon = 2.3 \times 10^3\ M^{-1}\ cm^{-1}$), 1655 ($7 \times 10^2$). ^1H NMR (CD_2Cl_2): δ 2.78 (s, 3H, C(O)CH_3), 7.6−7.9 (m, 20H, $AsPh_4^+$). ^{13}C NMR (CD_2Cl_2): δ 161.1 (*C*O), 199.3 (*C*(O)CH_3), 135.5, 133.5, 131.9 (Ph, *C*H), 51.0 (C(O)*C*H_3). A crystal suitable for single-crystal X-ray diffraction was selected and the structure determined. At convergence, R1 = 0.0316 and GOF = 1.043 for 327 variables refined against 6788 reflections with $I > 2\sigma$.

[Ir(C(O)CH$_3$)(μ-I)(CO)I$_2$]$_2$[AsPh$_4$]$_2$ ($AsPh_4^+$ salt of 4). *fac*-$[CH_3Ir(CO)_2I_3][AsPh_4]$ (205 mg, 0.2 mM) was dissolved in 25 mL of acetonitrile under argon atmosphere. The solution was then subjected to bulk photolysis until species **1a** was no longer detected by IR spectroscopy (about 2 h). The solvent was removed in vacuo, and then the residue was dissolved in 10 mL of CH_2Cl_2 under argon. By layering the CH_2Cl_2 solution with Et_2O, dark orange-red crystals were obtained. Anal. Calcd for ($C_{54}H_{46}O_4Ir_2I_6As_2$): C, 31.57; H, 2.26. Found: C, 31.50; H, 2.33. IR (KBr) ν(CO) cm^{-1}: 2046sh, 2034vs, 2009s, 1670sh, 1650s, 1637sh; IR (CH_2Cl_2) ν(CO) cm^{-1}: 2094w, 2054sh, 2041vs, 1692wb, 1664wb. ^{13}C NMR (solid state): δ 159.7 (*C*O), 190.6 (*C*(O)CH_3), 137.1, 133.8, (Ph, *C*H), 120.7, (*C*As), 46.5 (C(O)*C*H_3). A crystal suitable for single-crystal X-ray diffraction was selected and the structure determined. At convergence, R1= 0.0478 and GOF = 1.060 for 309 variables refined against 5980 reflections with $I > 2\sigma$.

Ir(C(O)CH$_3$)(CO)(py)$_2$I$_2$] (5). Excess pyridine was added to a freshly photolyzed acetonitrile solution of **1a** leading to the preparation of species **4** under argon. By layering the reaction solution with Et_2O, $AsPh_4I$ soon separated as white crystals. From the remaining solution, bright orange crystals were obtained (few days). Anal. Calcd for ($C_{13}H_{13}O_2IrN_2I_2$): C, 23.12; H, 1.94; N, 4.15. Found: C, 23.44; H, 1.92; N, 3.99. IR (CH_2Cl_2) ν(CO) cm^{-1}: 2053vs, 1662s. ^1H NMR (CD_2Cl_2): δ 2.9 (s, 3H, C(O)CH_3); 7.3 (q), 7.6−7.9 (m), 8.8 (d) and 9.1 (d). ^{13}C NMR (CD_2Cl_2): δ 197.0 (*C*(O)CH_3), 157.0 (*C*O); 139.5, 126.2, 125.1 (Py, *C*H); 52.0 (C(O)-*C*H_3). A crystal suitable for single-crystal X-ray diffraction was selected and the structure determined. At convergence, R1 = 0.0237 and GOF = 1.028 for 183 variables refined against 3981 reflections with $I > 2\sigma$.

Table 1. Parameters of X-ray Diffraction Data Collections and Structure Determinations[a]

structure	1	2	5
formula	$C_{28}H_{23}O_3AsI_3Ir$	$C_{54}H_{46}O_4As_2I_6Ir_2$	$C_{13}H_{13}N_2O_2I_2Ir$
a (Å)	10.885(5)	10.528(2)	10.0999(4)
b (Å)	13.069(6)	12.052(2)	
c (Å)	13.452(7)	12.423(2)	17.2639(7)
α(°)	63.893(7)	71.549(2)	90
β(°)	66.249(7)	85.826(2)	106.762(1)
γ(°)	85.134(8)	70.565(2)	90
V(Å^3)	1563(1)	1409.2(3)	1678.8(1)
Z	2	1	4
fw	1055.28	2054.54	675.25
D_{calc} (g/cm^3)	2.242	2.421	2.672
μ(cm^{-1})	80.311	92.11	116.33
space group	triclinic $P\bar{1}$	triclinic $P\bar{1}$	monoclinic $P2_1/n$
color	dark brown	orange	dark yellow
size (mm^3)	0.3 × 0.25 × 0.1	0.2 × 0.15 × 0.1	0.15 × 0.1 × 0.05
temp (K)	293	110	117
Mo Kα λ(Å)	0.71073	0.71073	0.71073
T_{min}/T_{max}[b]	0.587	0.670	0.648
θ range (°)	$1.75 \le \theta \le 28.25$	$2.29 \le \theta \le 28.02$	$2.11 \le \theta \le 28.71$
	$-13 \le h \le 12$	$-13 \le h \le 12$	$-13 \le h \le 12$
	$-16 \le k \le 17$	$-15 \le k \le 15$	$-12 \le k \le 13$
	$-16 \le l \le 16$	$-16 \le l \le 15$	$-20 \le l \le 21$
total reflns/ unique reflms	13 130/6788	10 838/5980	14 505/3981
	$R_{int} = 0.0291$	$R_{int} = 0.0306$	$R_{int} = 0.0310$
variables	327	309	183
R [$I > 2\sigma(I)$]	R1 = 0.0316	R1 = 0.0478	R1 = 0.0237
	wR2 = 0.0772	wR2 = 0.1270	wR2 = 0.0559
GOF	1.043	1.060	1.028

[a] Structure **1**: The $AsPh_4^+$ salt of **2a**: *mer,trans*-$[Ir(C(O)CH_3)(CO)_2I_3][AsPh_4]$. Structure **2**: The $AsPh_4^+$ salt of **4**: $[Ir(C(O)CH_3)(CO)I_3]_2[AsPh_4]_2$. Structure **5**: *mer,trans*-$[Ir(C(O)CH_3)(CO)(py)_2I_2]$. [b] The transmission ratio was from absorption correction using program SADABS.

Crystal Structures. Crystallographic data were collected using a Bruker CCD platform diffractometer. The SMART program (Bruker AXS, Inc.) was used to determine the unit cell parameters and data collection (30 s/frame, 0.3°/frame for a sphere of diffraction data). The data were collected at room and low temperature. The raw frame data were processed using the SAINT program (Bruker AXS, Inc.). The absorption correction was applied using the SADABS program (Bruker AXS, Inc). Subsequent calculations were carried out using the SHELXTL program (Bruker AXS, Inc.). The structure was solved by direct methods and refined on F^2 by full-matrix least-squares techniques. All hydrogen atoms were located theoretically. The detailed information of data collections and structure determinations are listed in Table 1. Other crystal data and cell packing for the structures of *mer,trans*-$[Ir(C(O)CH_3)(CO)_2I_3][AsPh_4]$, the dimer $[Ir(C(O)CH_3)(CO)I_3]_2][AsPh_4]_2$, and *mer,trans*-$[Ir(C(O)CH_3)(CO)(py)_2I_2]$ are presented in the Supporting Information Figures S1−S3 and Tables S1−S3.

Computations. DFT calculations were performed at B3LYP theory level using the LACVP* polarized basis set. Geometries were optimized inside the Titan software suite (Wavefunction, Inc.). Except where noted, optimizations were calculated as singlet ground states due to significant HOMO−LUMO gaps (>3 eV), without any symmetry constraints and represent structures in the gas phase.

Results and Discussion

Photolysis Studies. Figure 1 displays the changes in the IR spectrum of a DCE solution of the *fac*-$[CH_3Ir(CO)_2I_3]^-$

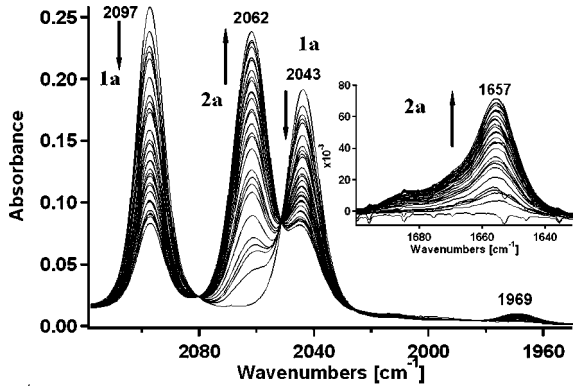

Figure 1. FTIR spectral changes (ν_{CO} region) for a DCE solution of the $AsPh_4^+$ salt of **1a** (1.3 mM) under 1.0 atm of CO (298 K) as the result of continuous photolysis at 366 nm. Successive spectra over the first 150 s were recorded after 5 s intervals of irradiation in a CaF_2 IR cell (0.1 cm path length). (The band at 1969 cm^{-1} denotes the appearance of the *cis*-$[Ir(CO)_2I_2]^-$ anion in the later stages.)

anion (**1a**) (1.3 mM as the $AsPh_4^+$ salt) during photolysis under CO (1 atm) at ambient temperature using the excitation wavelength (λ_{irr}) 366 nm. A 3D representation of these data appears in the Supporting Information as Figure S4. In these figures, the absorption bands of **1a** at 2097 and 2043 cm^{-1} (ϵ = 1900 and 1300 M^{-1} cm^{-1}, respectively) decrease smoothly with concomitant growth of two new absorption bands at 2062 and 1657 cm^{-1} (ϵ = 2300 and 700 M^{-1} cm^{-1}, respectively, determined from the isolated and well-characterized product). Isosbestic points are clearly evident at 2080 and 2051 cm^{-1}.

On the basis of FTIR, NMR, and ESI-MS spectroscopic analysis, the photoproduct was identified as the *mer*,*trans*-$[Ir(C(O)CH_3)(CO)_2I_3]^-$ anion (**2a**) (eq 1). The FTIR bands at 1657 and 2062 cm^{-1} can be assigned, respectively, to the stretching mode of the acyl carbonyl and antisymmetric stretching modes of the trans terminal carbonyls. The structure of **2a** was confirmed by isolating the $AsPh_4^+$ salt in a bulk photolysis experiment and determining the X-ray crystal structure (Figure 2). The structure of the corresponding *fac*-isomer **2b** was recently reported.[4e]

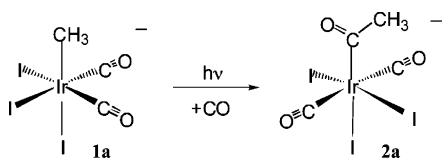

(1)

The quantum yield for appearance of the product **2a** was calculated by monitoring the strongest absorption changes at 2062 cm^{-1} and plotting the incremental quantum yield, Φ_i, versus time over the early stages of the reaction in DCE solutions (see Experimental Section).[8c,d] Extrapolation of this plot to the *y* intercept accounted for inner-filter effects (absorbance at 366 nm changed during experiment) and gave a Φ_{2a} of 0.045 ± 0.002, reproducible over multiple measurements. The quantum yield for disappearance of **1a** (Φ_d) is (within experimental uncertainty) the same as that for the appearance of **2a**, as is evident from the spectral changes in Figure 1.

Continued photolysis (λ_{irr} = 366 nm) of such solutions under CO for >10 h revealed a secondary photolysis process

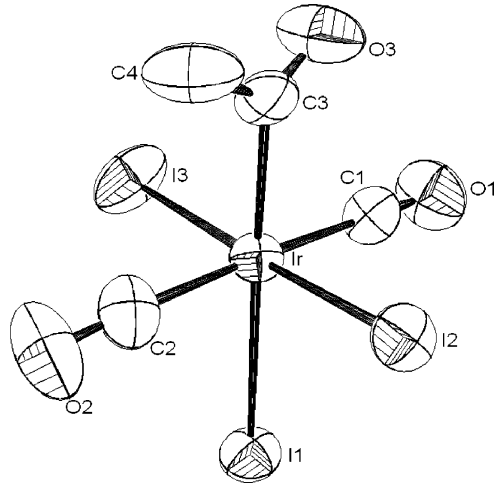

Figure 2. Structure of **2a** (counterion and hydrogens omitted for clarity, ellipsoid probability at 50%). Selected bond lengths (Å) are Ir−C(1) = 1.951(6), Ir−C(2) = 1.911(7), Ir−C(3) = 2.125(6), C(1)−O(1) = 1.099(7), C(2)−O(2) = 1.126(7), C(3)−O(3) = 1.146(7), C(3)−C(4) = 1.440(8), Ir−I(1) = 2.8144(11), Ir−I(2) = 2.6792(90), and Ir−I(3) = 2.6902(10). Selected angles (deg) are O(1)−C(1)−Ir = 178.7(5), O(2)−C(2)−Ir = 175.0(5), O(3)−C(3)−Ir = 118.5(4), and C(4)−C(3)−Ir = 117.1(4).

involving the slow formation of the *cis*-$[Ir(CO)_2I_2]^-$ anion (ν(CO) bands at 2044 and 1969 cm^{-1} in ambient DCE, eq 2). The net reaction is acetyl iodide reductive elimination, although it is uncertain whether this photoinduced process occurs directly from **2a**, which is thermally stable under these conditions, or from its isomer *fac*-$[Ir(C(O)CH_3)(CO)_2I_3]^-$ (**2b**) (see below).

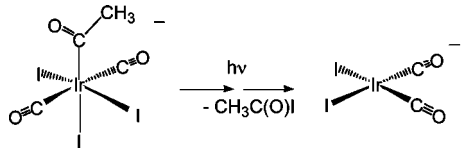

(2)

Photolysis of **1a** as the $AsPh_4^+$ salt in ambient THF under CO showed similar results but with a higher degree of reductive elimination of acetyl iodide to yield *cis*-$[Ir(CO)_2I_2]^-$ [IR (THF) ν(CO): 2037vs, 1959vs]. When **1a** was photolyzed in ambient acetonitrile under CO, additional species showing ν_{CO} bands were observed at 2083w and 2045s cm^{-1} together with the formation of **2a** (2055vs, 1648w,b cm^{-1}) and *cis*-$Ir(CO)_2I_2^-$ (2043s and 1969s cm^{-1}).

The course of the photochemical reaction of **1a** was also studied by ^1H NMR in CD_3CN. After 15 min of photolysis in an argon-filled NMR tube, some unreacted **1a** (δ 2.100, s, CH_3), remained but about three times as much of an acetyl species (δ 2.575, s, C(O)CH_3) was present. When excess ^{13}CO was added at ambient temperature, the mono-labeled **2a** *mer*,*trans*-$[Ir(C(O)CH_3)(CO)(^{13}CO)I_3]^-$ was observed and characterized by NMR (^1H NMR: δ 2.78 (s, 3H, C(O)CH_3), ^{13}C NMR: δ 161.1 (*C*O)) and by ESI-MS (673.70 *m*/*z* (M^-)). Thus, the spectroscopic data strongly suggest that, in the presence of acetonitrile, a solvent-stabilized acyl anionic complex $[Ir(C(O)CH_3)(CO)(AN)I_3]^-$ is generated photochemically.

Continuous photolysis (λ_{irr} = 366 nm) of **1a** (2.5 mM) in DCE solution under an inert atmosphere (Ar) led to different IR spectral changes (Figure 3) than those seen under CO.

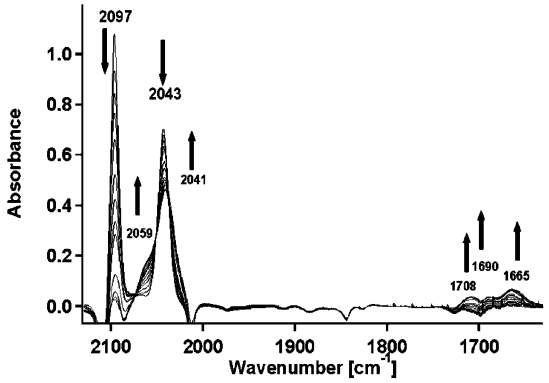

Figure 3. FTIR spectra (ν_{CO} region) tracking the continuous photolysis (366 nm) of **1a** as a $AsPh_4^+$ salt (2.5 mM) in DCE solution under Ar (1 atm). (298 K, 0.2 cm path length, IR cell).

Within a few minutes, new IR absorption bands appeared that overlapped the 2043 cm^{-1} band characteristic of **1a**. In addition, three broad and weaker bands between 1665 and 1708 cm^{-1} were detected. The quantum yield for the disappearance of **1a** under these conditions (0.072 ± 0.004) was evaluated by monitoring the IR absorption changes at 2097 cm^{-1} and plotting Φ_i versus time to correct for inner-filter effects.

Longer-term photolysis of acetonitrile solutions of the $AsPh_4^+$ salt of **1a** (2 h) under argon gave a solution for which the IR spectrum displayed ν(CO) absorptions at 2100w, 2059sh, 2041s, 1708w,b, 1690w,b, and 1665w,b cm^{-1}. These bands were assigned to a mixture of the anionic acetyl iridium dimers, $[Ir(C(O)CH_3)(\mu\text{-}I)(CO)I_2]_2^{2-}$, one of which, **4**, was isolated as a $AsPh_4^+$ salt and the crystal structure determined (Figure 4). The electron density map indicated the carbonyl (C3, O2) and iodo (I1) ligands to have disorder, which can be treated as two isomers (Figure 4a and b) regarding the orientations of carbonyl and iodo in the axial sites. By constraining the equal thermal parameters of C3, O2, and I1 in two isomers, the refinement derived occupancies of 81.8:18.2 for the two isomers.

When a solution of the dimers generated by photolysis under argon in ambient dichloromethane was exposed to excess CO, the resulting IR spectral changes indicated the formation of the mononuclear *mer*,*trans*-$[Ir(C(O)CH_3)(CO)_2I_3]^-$ anion **2a**. Careful IR subtraction spectra analysis during the reaction also revealed appearance of a weak, but sharp, positive absorption at 2112 cm^{-1} that can be attributed to formation of the fac,cis isomer **2b** (eq 3). Similar reactions

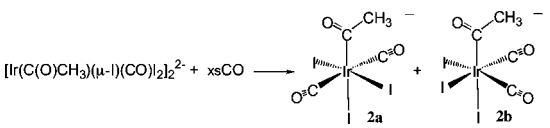

(3)

with CO and other ligands have been reported for analogous rhodium dimers.[10]

An analogous photolysis of **1a** was carried out under argon in a NMR tube with CD_2Cl_2 as the reaction solvent. The product solution demonstrated two signals in the ^1H NMR spectrum at 2.63 and 2.54 ppm in an approximate 1:1 ratio consistent with the formation of acyl complexes, presumably the dimers. After addition of excess ^{13}CO to the photolyzed solution, singly labeled **2a** *mer*,*trans*-$[Ir(C(O)CH_3)(CO)(^{13}CO)I_3]^-$ proved to be the only detectable isotopically enriched species in the ^{13}C NMR spectrum.

When excess pyridine was added to a CH_2Cl_2 solution of the dimers generated under argon, the product was the neutral bis(pyridine) complex **5** (eq 4). This was isolated in almost

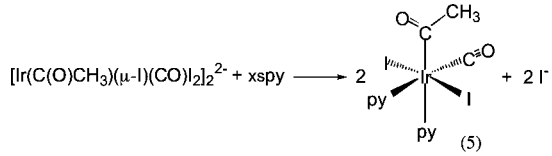

(4)

quantitative yield, and the X-ray crystal structure was determined (Figure 5). It is likely that the formation of **5** proceeds by breaking the weak bridging iodide bond trans to acetyl group followed by substitution of the iodide trans to CO by a second pyridine ligand. The rhodium analogue of **5** was recently reported, but the structure was not determined.[10b]

As noted above, the iridium(I) anion, *cis*-$Ir(CO)_2I_2^-$, was observed as a product in the long-term photolysis of DCE solutions of **1a** under CO, although the *mer*,*trans*-$[Ir(C(O)CH_3)(CO)_2I_3]^-$ anion (**2a**) is the principal product formed initially. In this context, DCE solutions were prepared from the isolated $AsPh_4^+$ salt of **2a** (1.5 mM) in order to investigate the photochemistry of this species directly and to evaluate whether *cis*-$Ir(CO)_2I_2^-$ might result from the

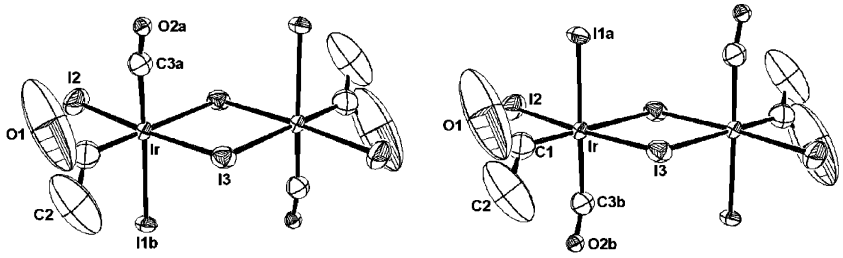

Isomer **4a** Isomer **4b**

Figure 4. (a) and (b). Structure of **4** (counterion and hydrogens omitted for clarity; ellipsoid probability at 50%). The observed disorder between the iodo and carbonyl ligands in the axial sites is shown in (a) and (b). Selected bond lengths (Å) are Ir−C(1) = 1.995(16), Ir−C(3A) = 1.854(10), Ir−C(3B) = 2.07(5), C(1)−O(1) = 1.183(10), C(3A)-O(2A) = 1.061(9), C(3B)-O(2B) = 1.089(10), C(1)−C(2) = 1.364(10), Ir−I(1A) = 2.642(4), Ir−I(1B)= 2.6949(10), Ir−I(2) = 2.6769(9), Ir−I(3) = 2.6905(8), and Ir(1)−I(3) = 2.8639(10). Selected angles (deg) are Ir−I(3)−Ir(1) = 93.33(2), I(2)−Ir−I(3) = 175.77(3), C(3A)−Ir−I(1B) = 177.7(4), C(1)−Ir−I(3) = 94.5(4), C(1)−Ir−I(2) = 89.1(4), O(1)−C(1)−Ir = 119.1(15), and C(2)−C(1)−Ir = 130.7(17).

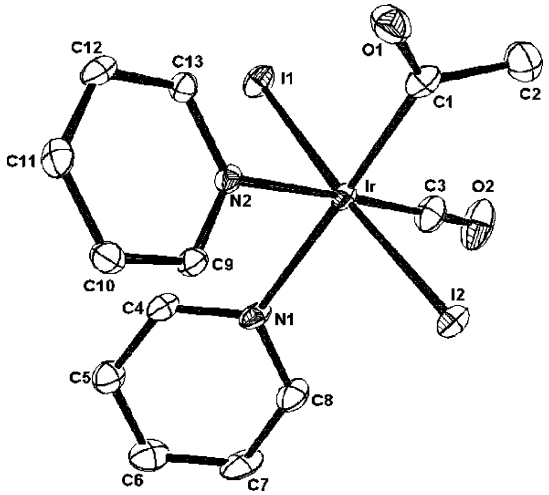

Figure 5. Structure of $Ir(C(O)CH_3)(CO)(py)_2I_2$ (**5**). (Hydrogen atoms omitted for clarity; ellipsoid probability at 50%) Selected bond lengths (Å) are Ir−C(1) = 2.048(4), Ir−C(3) = 1.861(4), Ir−I(1) = 2.6739(4), Ir−I(2) = 2.6774(4), C(1)−O(1) = 1.210(5), C(3)−O(2) = 1.122(5), C(1)−C(2) = 1.285(19), Ir−N(1) = 2.255(3), and Ir−N(2) = 2.146(3). Selected angles (deg) are O(1)−C(1)−Ir = 121.4(3), C(2)−C(1)−Ir = 120.3(3), O(2)−C(3)−Ir = 178.5(4), I(1)−Ir−N(1) = 91.00(9), I(1)−Ir−N(2) = 91.71(9), and N(2)−Ir−N(1) = 85.28(12).

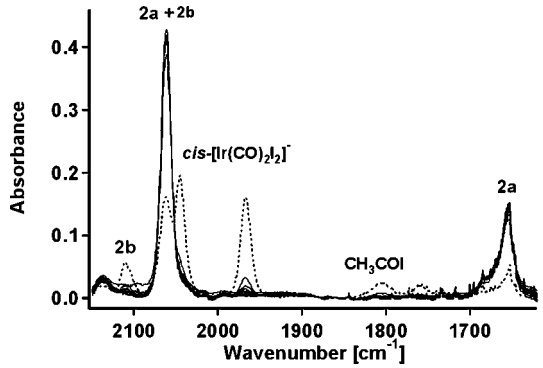

Figure 6. FTIR spectra (ν_{CO} region) tracking the continuous photolysis (366 nm) of **2a** as a $AsPh_4^+$ salt of (1.5 mM) under CO (1 atm) in DCE (298 K): 0 and 2 h, solid lines; 16 h, dotted line. The bands attributed to formation of **2b** and to *cis*-$[Ir(CO)_2I_2]^-$ are indicated.

secondary photolysis of **2a**. Irradiation of these solutions at 366 nm under CO (1.0 atm) at ambient temperature led to the IR and UV−vis spectral changes reported in Figure 6 and in Supporting Information Figure S5, respectively. These indicate that both *cis*-$Ir(CO)_2I_2^-$ and the *fac*-$[Ir(C(O)CH_3)(CO)_2I_3]^-$ anionic isomer **2b**, as well as acetyl iodide, are formed; however, the net photoreactivity of **2a** ($\Phi \leq 0.007$) is about an order of magnitude less than that of **1a**. Although the spectral changes are somewhat ambiguous, we speculate that **2b** is the likely predecessor of *cis*-$Ir(CO)_2I_2^-$. Concerted thermal or photochemical reductive elimination from **2a** should give the less-stable *trans*-$Ir(CO)_2I_2^-$, although one might speculate on other photoreaction scenarios.

Comments on the X-ray Crystal Structures. The structure of the *mer*,*trans*-$[Ir(C(O)CH_3)(CO)_2I_3]^-$ anion (**2a**, Figure 2) can be compared to that of the fac,cis isomer **2b**, recently reported by Haynes et al.[4e] The influence of the acyl group is reflected in the longer Ir−I bond trans to acetyl group. For each structure, this bond is longer (by ∼0.1 Å) than the Ir−I bond cis to the acetyl group, which in **2a** is trans to another iodide but in **2b** is trans to a carbonyl. The trans influence of the acyl is also evident in the structure of *mer*,*trans*-$[Ir(C(O)CH_3)(CO)(py)_2I_2]$ (**5**, Figure 5), which shows the Ir−N bond trans to the acyl to be 0.1 Å longer than that trans to the carbonyl.

The crystal structure determined for the dimeric anion $[Ir(C(O)CH_3)(\mu\text{-}I)(CO)I_2]_2^{2-}$ (**4**, Figure 4) shows disorder in the axial sites for both Ir(III) centers. It is not clear whether this indicates the presence of two closely related dimers that have co-crystallized or is simply the disorder in the cellular packing of a single species. (The refined structure included ∼18% disorder for the centro-symmetric isomer.) The former is consistent with the observation that the IR spectrum of the isolated solid displays two acetyl carbonyl ν_{CO} bands, indicating the presence of at least two isomers in the isolated solid. The disorder suggests that co-crystallization of species with the axial CO oriented on the same side of the diiodo bridges with another species having the COs on opposite sides. In other respects, the structure of **4** resembles that of an analogous dinuclear rhodium(III) compound.[11] The iridium atoms show a distorted octahedral arrangement, and the two octahedra are linked together by a double iodide bridge across an apparent center of symmetry. The iridium-bridging iodide distances are 2.6905(9) and 2.8639(10) Å, in line with the trans influence of the acyl group. The variation in the Ir−iodide bridge distances is similar to that observed for the Rh−iodide bridges in $[Rh(C(O)CH_3)(\mu\text{-}I)(CO)I_2]_2[Me_3PhN]_2$.[11,12]

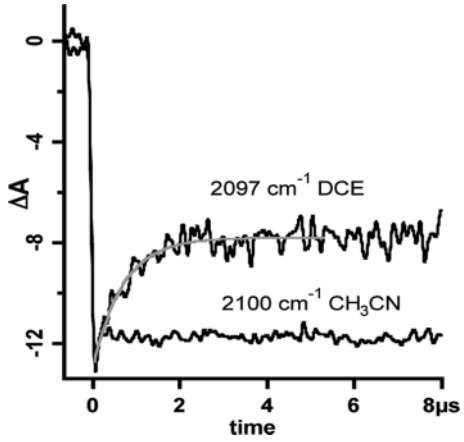

Figure 7. Absorbance change at 2097 (DCE) and 2100 cm^{-1} (CH_3CN) following 355 nm laser flash photolysis of a 3 mM sample solution of **1a** as the $AsPh_4^+$ salt in the presence of CO 60 psig at 298 K. (The absorbance changes shown are in mO.D. units.)

Laser Flash Photolysis Studies. Figure 7 displays the temporal absorbance of the 2097 cm^{-1} ν_{CO} band of *fac*-$[CH_3Ir(CO)_2I_3]^-$ (3 mM in DCE solution, 60 psig CO at 25 °C)

(10) (a) Adams, H.; Bailey, N. A.; Mann, B. E.; Manuel, C. P.; Spencer, C. M.; Kent, A. G. *J. Chem. Soc., Dalton Trans.* **1988**, 489−496. (b) Haynes A.; Maitlis, P. M.; Stanbridge, I. A.; Haak, S.; Pearson, J. M.; Adams, H.; Bailey, N. A. *Inorg. Chim. Acta* **2004**, *357*, 3027−3037.

(11) Adamson, G. W.; Daly, J. J.; Forster, D. *J. Organomet. Chem.* **1974**, *71*, C17−C19.

(12) Evans, J. A.; Russell, A. B.; Shaw, B. L. *Chem. Commun.* **1971**, 841−842.

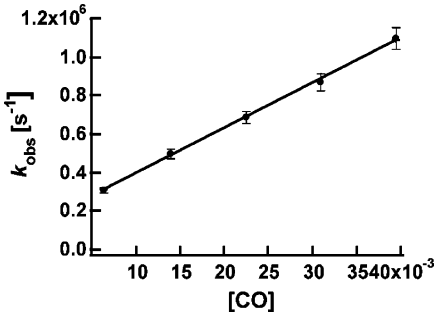

Figure 8. Plot of k_{obs} vs [CO] for re-formation of **1a**, monitored at 2097 cm^{-1} (298 K, DCE).

following 355 nm pulse laser excitation. This IR band undergoes an immediate bleach followed by partial recovery that can be fit to an exponential function to give the first-order rate constant $k_{obs} = 8.7\ (\pm 0.2) \times 10^5\ s^{-1}$. Varying [CO] over the range 6−40 mM[13] leads to increases in the reformation rate for **1a** but does not change the magnitude of the initial bleaching *nor the quantitative amount of recovery*. The same figure also displays the temporal behavior at 2100 cm^{-1} (ν_{CO} max) resulting from flash photolysis of **1a** in acetonitrile under analogous conditions. In the latter case, there is little recovery on the microsecond time scale of the experiment. Such solvent-dependent behavior is consistent with initial formation of an unsaturated intermediate via ligand photodissociation followed by trapping of that species by coordination to a solvent molecule. Acetonitrile would bind more strongly than would DCE, hence any reaction with CO, or another ligand, would be much more sluggish in acetonitrile.

The possible role of reversible iodide dissociation in the generation and decay of the transient bleaching of **1a** in DCE was probed by conducting further flash photolysis experiments in the presence of added $[Bu_4N]I$ (15−30 mM). The excess I^- had no effect on the rate or on the extent of **1a** regeneration, so it was concluded that iodide photodissociation is not playing a role in this case.

A plot of the k_{obs} vs [CO] (298 K) proved to be linear with a nonzero intercept (Figure 8). This behavior strongly suggests that at least one of the intermediates initially formed upon flash photolysis ($\mathbf{I_{CO}}$) is the result of CO photodissociation. The second-order rate constant for the reaction of CO with $\mathbf{I_{CO}}$ (eq 5)[14] would be derived from the equation

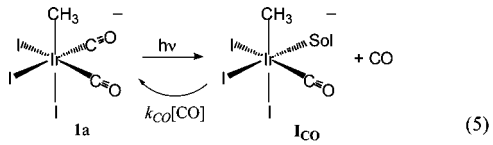

(5)

$k_{obs} = k_{CO}[CO] + k_M$ used to fit the data in Figure 8, which gave the values $k_{CO} = 2.50\ (\pm 0.05) \times 10^7\ M^{-1}\ s^{-1}$ and $k_M = 1.6\ (\pm 0.1) \times 10^5\ s^{-1}$. The nonzero intercept (k_M) suggests that there is also a CO-independent pathway for the re-formation of **1a.** This will be discussed further.

As noted above, the ratio of the overall absorbance bleach (2097 cm^{-1} band) at long time (ΔA_∞) relative to the prompt absorbance bleach (ΔA_o) was independent of [CO], the experimental $\Delta A_\infty/\Delta A_o$ value being 0.64 (± 0.02). This indicates that other intermediates besides $\mathbf{I_{CO}}$ are formed in the photoreaction or that competing processes deplete $\mathbf{I_{CO}}$ by pathways that are also first order in [CO] but lead to different products. The first alternative, namely that several intermediates are formed, receives support from the TRIR spectrum recorded (point by point) immediately following flash photolysis of a DCE solution of **1a** under argon (Supporting Information Figure S6). A mono-carbonyl complex such as $\mathbf{I_{CO}}$ should display a single ν_{CO} band; however, weak absorptions were seen at 2156, 2116−2110, 2075, 2059, and 1665 cm^{-1} and a stronger one at 2032 cm^{-1}. Since the bleach of the 2043 cm^{-1} band of **1a** proved to be about half that expected given the magnitude of the bleach at 2097 cm^{-1}, it appears likely that another transient band of moderate strength appears at ∼2040 cm^{-1}. From these data, it is clear that several intermediates are formed in the flash photolysis of **1a**.

One such intermediate would be an acyl complex formed by methyl migration to a cis carbonyl as a reactive pathway from the initial excited state (ES), in competition with deactivation to **1a** and with CO dissociation to give $\mathbf{I_{CO}}$. Trapping by solvent would give an acyl species, $\mathbf{I_M}$, which in the absence of CO would be expected to decay back to **1a** (eq 6).[14] In the presence of CO, formation of **2b** is likely.

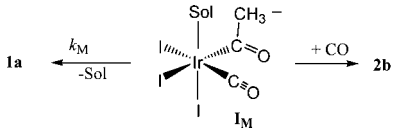

(6)

Since only about one-third of the **1a** depleted by the flash is regenerated, it is necessary to account for the remaining material and to evaluate pathways leading to the formation of **2a**. As noted above, continuous photolysis under argon leads primarily to formation of the dimers of the acyl carbonyl triiodide anions, $[Ir(C(O)CH_3)(\mu\text{-}I)(CO)I_2]_2^{2-}$. The $AsPh_4^+$ salt of **4** was isolated and characterized structurally, but the IR spectra suggest that other isomers are also present. These could be formed via dimerization of $\mathbf{I_M}$ (with appropriate loss of solvent) or by trapping of $\mathbf{I_M}$ by other monomers. However, since CO addition to $\mathbf{I_M}$ would give **2b** rather than **2a**,[14] another intermediate, such as $\mathbf{I_{M-mer}}$ is a likely precursor to the latter (eq 7). Reaction of $\mathbf{I_{M-mer}}$ with CO would give **2a**, while reverse migration of CH_3- to the metal would give the mer isomer **1b**. Although **1b**

(13) Cargill R. W. *Carbon Monoxide*, 1st ed.; IUPAC Solubility Data Series Vol. 23; Pergamon Press: Elmsford, NY, 1990.

(14) (a) In discussing the reactions of the thermal substitution reactions of the hexacoordinate iridium(III) organometallic compounds, it will be assumed that these occur with retention of configuration, as has generally been seen in the ligand substitution reactions of other $4d^6$ and $5d^6$ complexes. (b) It should be noted that, in earlier flash photolysis studies of acyl carbonyl complexes of manganese and cobalt,[7b−f] intermediates seen in weakly coordinated solvents were concluded to have η^2-acyl coordination rather than forming the solvento species. In the present case, one should consider the possibility that, for species such as $\mathbf{I_M}$ and $\mathbf{I_{M-mer}}$, the vacated coordination site may be lightly stabilized not by solvent coordination but by such η^2-acyl interaction.

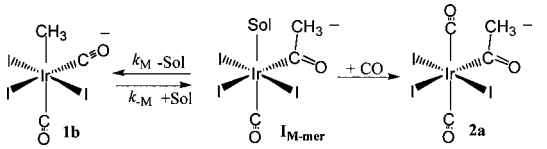

(7)

was not detected, this is consistent with the view that **1b** is reactive toward migratory insertion.[17]

Computational Studies. The complexity of the photoreaction results led us to employ DFT computations to seek insight into potential intermediates and prospective transformations. A key feature of the above discussion is that ligand photodissociation from a hexacoordinate species such as **1a** is accompanied by stereochemical lability of the coordination sphere. Although thermally induced ligand substitutions of $4d^6$ and $5d^6$ complexes generally occur by stereoretentive pathways, analogous photochemical reactions are often coupled to isomerizations.[15] The energy introduced by absorption of a UV−vis photon generally exceeds the metal−ligand bond energies, so dissociative ligand labilization is a likely electronic ES mechanism. The species formed by the CO dissociation from the ES of **1a** would be pentacoordinate and is likely to carry vibrational excitation in excess of any activation energy required for pseudorotation to other pentacoordinate isomers. This is illustrated in Scheme 2. Photodissociation of CO would first give a square pyramidal anion, $[CH_3Ir(CO)I_3]^-$ (**3a**), with the methyl group in the equatorial position, which might either be trapped by solvent to give $\mathbf{I_{CO}}$ or isomerize to the pentacoordinate anion **3b** which would react with solvent to give *mer*-$[CH_3Ir(CO)I_3(Sol)]^-$ ($\mathbf{I_{CO-mer}}$), a predecessor of **1b**. In the condensed phase, solvent trapping of the pentacoordinate intermediates is likely to be competitive with isomerizations, so a distribution of products is probable.

In this context, DFT computations were initiated to examine whether isomerization from **3a** to **3b** would be a reasonable expectation. It should be emphasized that these were carried out for gas-phase species and ignore both general and specific solvation effects. Given these qualifications, it is notable that the DFT calculations (summarized in Supporting Information Table S4) clearly show that **3a** has a strong tendency to rearrange to **3b**. Pseudorotation to the square pyramidal isomer with an axial methyl is calculated to be 22 kcal mol^{-1} downhill if both are singlet states. The triplet state of $[CH_3Ir(CO)I_3]^-$ optimizes to a trigonal bipyramidal geometry with the methyl group and two iodides in the equatorial positions (**3c**) with an energy very close to that calculated for **3a** (Table S4) Since that trigonal bipyramidal species would be a likely intermediate in the **3a** → **3b** transformation, the respective energies of **3a**, **3c**, and **3b** portends a ready pathway for such an isomerization.[16] Although the calculated energy difference between **3a** and **3b** seems surprisingly large, the trend is consistent with the model proposed previously for photoisomerization of rhodium(III) and iridium(III) complexes.[15] Trapping of **3b** by solvent would give $\mathbf{I_{CO-mer}}$, and reaction of the latter with CO gives **1b** with one carbonyl trans to the methyl group and one cis. It is this type of coordination that characterizes the species argued to be precursor to the C−C bond formation step of the Cativa cycle (Scheme 1).

Scheme 2. Hypothetical Species Formed upon Photochemical Excitation of **1a**

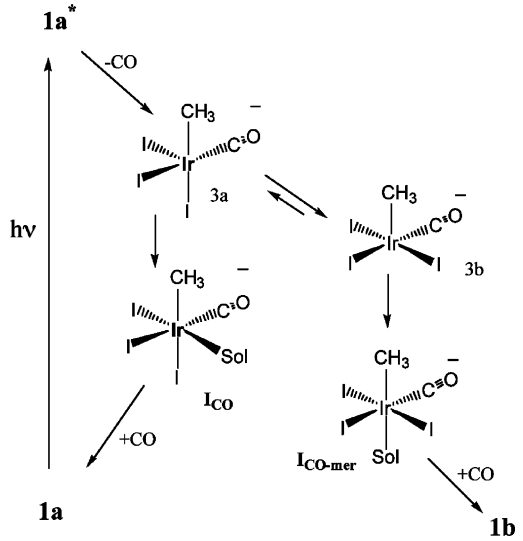

Solvent-assisted migratory insertion of **1b** to give $\mathbf{I_{M-mer}}$ followed by rapid reaction with CO leads to **2a**, the principal product of the photolysis of **1a** under CO. DFT calculations of **1b** and of a likely transition state for the migratory insertion reactions (Table S4) would suggest an activation energy of ∼16 kcal mol^{-1} for the first step in this sequence (eq 7). However, it should be reemphasized that the computations do not account for specific or general solvation effects. Attempts to account for such by coordinating a CH_2Cl_2 molecule to the iridium center in the transition state of the migration pathway only lowered the E_a by 2 kcal mol^{-1}, although a pathway involving the direct reaction between CO and $\mathbf{I_{CO-mer}}$ to give **2a** demonstrated a smaller E_a (∼10 kcal mol^{-1}). Notably, the calculated E_a in the absence of such interactions is in reasonable agreement with that (∼16 kcal mol^{-1}) computed by Kinnunen and Laasonen using DFT techniques for the same reaction.[17] These workers, furthermore, calculated the E_a for the analogous reaction of **1a** and demonstrated that the barrier to thermally induced migratory

(15) (a) Skibsted, L. H.; Strauss D.; Ford, P. C. *Inorg. Chem.* **1979**, *18*, 3171. (b) Skibsted, L. H.; Ford, P. C., *Inorg. Chem.* **1980**, *19*, 1828. (c) Talebinasab-Sarvari, M.: Ford, P. C. *Inorg. Chem.* **1980**, *19*, 2640, (d) Ford, P. C.; Wink, D.; DiBenedetto, J. *Prog. Inorg. Chem.* **1983**. *30*, 213−269. (e) In these studies, it was concluded that the pentacoordinated ES intermediate formed by ligand dissociation from the ligand-field ES of a d^6 hexacoordinate complex undergoes facile isomerization among various square pyramidal geometries before nonradiative deactivation and trapping by solvent to give substituted products. To a first approximation, the most favored configuration among these square pyramidal ES intermediates has the strongest π-donor ligand in the axial site (see ref 15c).

(16) (a) In an earlier study,[16b] ab initio calculations at the restricted Hartree−Fock level were used to probe the isomerizations between pentacoordinate iridium(III) complexes with two phosphine ligands, two hydrides and a π-donor ligand such as a halide. For such systems, facile isomerizations among the pentacoordinate singlet states apparently proceed via distorted trigonal bipyramidal structures that avoid the pseudo-D_{3h} structure, which is a higher-energy triplet species. This would appear not to be a problem in the present case. (b) Riehl, J.-F.; Jean, Y.; Eisenstein, O.; Pélissier, M. *Organometallics* **1992**, *11*, 729−737.

(17) Kinnunen, T.; Laasonen, K. *J. Mol. Struct. (THEOCHEM)* **2001**, *542*, 273−288.

Scheme 3. Proposed Pathways for Photoinduced Migratory Insertion

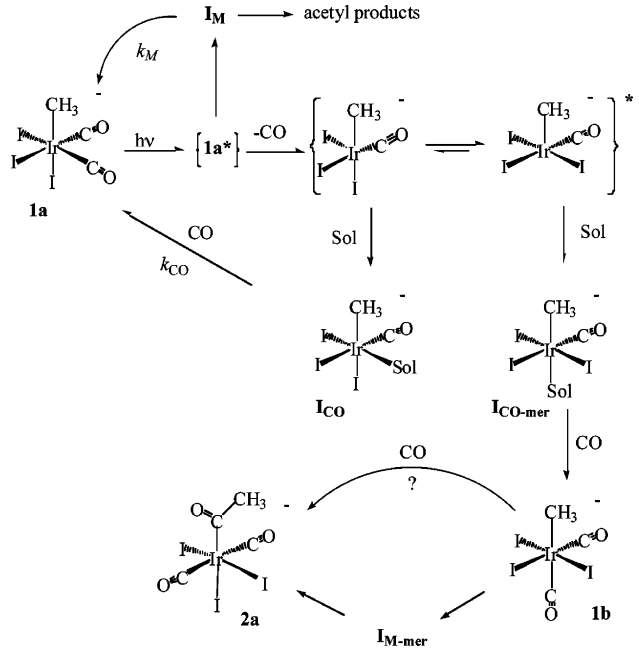

insertion of that species was ~12 kcal mol^{-1} higher. In the present study, it is shown that the photochemical labilization of CO, as well as the accompanying isomerization of the resulting five-coordinate intermediate, provides a pathway to coordination environments much more favorable to migratory insertion than the direct reaction of **1a**.

Summary. Scheme 3 draws together many of the observations and interpretations described above in the form of a proposed sequence of events following the ambient-temperature photoexcitation of the *fac*-$[CH_3Ir(CO)_2I_3]^-$ anion **1a**. In this scenario, the ES formed (probably a ligand-field (d → d) ES) is envisioned as having two reactive channels to deactivation, dissociation of CO from the ES to form a pentacoordinate species $\{CH_3Ir(CO)I_3^-\}$* or migratory insertion to carbonylate the Ir−CH_3 bond and give an acyl intermediate, $\mathbf{I_M}$, in what appears to be a lesser pathway.[18] In the absence of added CO, the latter undergoes the unimolecular reverse reaction to regenerate **1a** (the k_M pathway) and may be a contributor to the formation of the mixtures of dimers observed. In the presence of CO, $\mathbf{I_M}$ would be trapped to form **2b,** a possible precursor to the small amount of *cis*-$Ir(CO)_2I_2^-$ seen in Figure 1. The $\{CH_3Ir(CO)I_3^-\}$* intermediate is apparently labile toward isomerization between various geometric configurations; however, such isomerization is competitive with deactivation pathways concomitant with trapping by the solvent to form the lightly stabilized six-coordinate solvento species $\{CH_3Ir(CO)(Sol)I_3^-\}$, $\mathbf{I_{CO}}$ and $\mathbf{I_{CO-mer}}$. Of these, the former would react with CO to regenerate **1a** (the k_{CO} pathway), while the latter would react with CO to form **1b**. Under either Ar or CO atmospheres, the stable photoproducts generated are principally acyl complexes, dimers under inert atmosphere, **2a** under CO.

Dimers were not formed under argon in acetonitrile solutions. In this medium, the product was apparently the mononuclear species $[Ir(C(O)CH_3)(CO)(CH_3CN)I_3]^-$. Thus, we may conclude that such solvento acetyl complexes are the precursors to the dimeric acyl complexes formed in less-coordinating media. Flash photolysis studies also established that long-lived transient species are formed in acetonitrile solutions even under a CO atmosphere, consistent with the proposed formation of intermediates $\mathbf{I_{CO}}$ and $\mathbf{I_{CO-mer}}$ as the result of CO photodissociation.

A logical question is whether the photochemical investigations described here have relevance to the catalysis mechanisms for methanol carbonylation by related iridium iodo carbonyl complexes, given the markedly different conditions of the present studies. In detailed and very convincing mechanistic characterizations of the catalytic systems,[4e] it was demonstrated that, in contrast to the analogous rhodium catalyst for methanol carbonylation, migratory insertion pathways appeared to be rate limiting. Furthermore, catalysis was promoted by species that may serve to labilize I^- from Ir(III) iodo complexes and to sequester the iodide and by solvents that promote such iodide labilization. One conclusion of these studies is that replacing I^- by CO in the Ir(III) activates those COs positioned appropriately to participate in migratory insertion to form the acetyl intermediates that are precursors to $CH_3C(O)I$ elimination and hydrolysis to acetic acid. Nothing in the present study disputes those arguments. However, our results suggest that I^- labilization may not be a requirement for facile migratory insertion to form acyl Ir(III) complexes. Instead, the facility of acetyl formation appears to be greatly enhanced by photoinduced-diisomerization of **1a** to **1b**; thus, it may be largely dependent on the orientation of other ligands relative to the methyl and carbonyl groups participating directly in formation of the acyl group.

Acknowledgment. This research was supported by a grant (DE-FG02-04ER15506) from the Division of Chemical Sciences, Office of Basic Energy Research, U.S. Department of Energy.

(18) (a) A referee has suggested that intramolecular migratory insertion reactions for the ESs generated upon photolysis of **1a** may find some analogy in the oxidatively induced migratory insertion reactions described some years ago by Giering et al.[18b] In this context, one might consider whether the reactive ES(s) somehow mimic an intermediate induced by a redox reaction, or is the migratory insertion chemistry induced by radical pathways? We discount the latter on the basis of the high reproducibility of quantum yield measurements for the formation of the acyl species **2a**, which argues against any type of chain process. With regard to the former, we interpret the net photochemical transformations as being largely the result of ligand photolabilization, owing to the formation of ligand-field ESs of these d^6 complexes. Nonetheless, even ligand-field excitation involves formation of a hole in a previously filled π-bonding MO (as well as electronic population of a σ-antibonding MO),[15d] so a LF ES has (to this extent) some analogy to the product of a one-electron oxidation (or reduction) of the species in question. In this context, any migratory insertion occurring directly from such a ligand-field ES may find some analogy in the Giering experiment. (b) Prock, A.; Giering, W. P.; Greene, J. E.; Meirowitz, R. E.; Hoffman, S. L.; Woska, D. C.; Wilson, M.; Chang, R.; Chen, J. *Organometallics* **1991**, *10*, 3479−3485; Woska, D. C.; Wilson, M.; Bartholomew, J.; Eriks, K.; Prock, A.; Giering, W. P. *Organometallics* **1992**, *11*, 3343−3352; Woska, D. C.; Bartholomew, J.; Greene, J. E.; Eriks, K.; Prock, A.; Giering, W. P. *Organometallics* **1993**, *12*, 304−309.

Supporting Information Available: Cell packing diagrams for three crystal structures plus several relevant figures showing spectra; tables with listings of complete structure refinement details, bond lengths, and angles, anisotropic displacement parameters for non-hydrogen atoms, and hydrogen coordinates and isotropic displacement parameters; and a table of results of computational studies. This material is available free of charge via the Internet at http://pubs.acs.org.

IC0513033